How to cite: *Angew. Chem. Int. Ed.* **2025**, *64*, e202412669
doi.org/10.1002/anie.202412669

Membranes

Electrochemical identification and quantification of through-plane proton channels in graphene oxide membranes

Yiqing Wang and Siegfried Eigler**

Abstract: Stacked graphene oxide (GO) proton membranes are promising candidates for use in energy devices due to their proton conductivity. Identification of through-plane channels in these membranes is critical but challenging due to their anisotropic nature. Here, we present an electrochemical reduction method for identifying and quantifying through-plane proton channels in GO membranes. The simplicity lies in the operando optical observation of the change in contrast as GO is electrochemically reduced. Here, we find three proton-dominated three-phase interfaces, which are critical for the reduction reactions of GO membranes. Based on these findings, a method is proposed to identify and quantify through-plane channels in stacked GO proton membranes using a simple three-electrode device in combination with real-time imaging of the membrane surface.

Proton exchange membranes are important key components for the development of a new generation of energy devices, such as proton exchange membrane fuel cells or redox flow batteries.[1] In addition, proton exchange membranes have been used in reactors for the electrochemical synthesis of specific products.[2] In this context, two-dimensional (2D) materials have been studied as proton exchange membranes. Some 2D materials exhibit promising proton conductivity, such as $CdPS_3$ nanosheets and others.[3] GO is a unique material with hydrophilic surface functional groups, which possesses excellent gas barrier properties, making GO stacked membranes an ideal candidate for proton exchange membranes.[1–2,4] Proton transport in GO multilayers is faster than in monolayers.[5] In 2013, pure stacked GO membranes were used for the first time in fuel cells with proton conductivity values similar to Nafion membranes.[6] However, the high-tortuosity through-plane channels in stacked GO membranes, which are several orders of magnitude longer than the membrane thickness, makes proton transport performance in through-plane direction much lower than in-plane transport.[4,7] To mitigate the anisotropy in proton transport between through-plane and in-plane directions, researchers have proposed the construction of multidirectional proton conduction channels.[8] Although through-plane proton conductivity in GO membranes has been tested using a complex and environmentally demanding impedance analyzer-coupled membrane test system,[4,8a] efficient low-tortuosity through-plane channels (abbreviated in the text as through-plane channels) have not been effectively identified.[11] In order to screen high-performance GO proton membranes more efficiently, it is essential to explore simpler and more direct methods for identifying efficient through-plane channels.[9]

Electrochemical reduction of GO is well studied and reduced GO is formed.[10] Protons and electrons are directly involved in the reaction during the reduction process, as shown in the following reaction equation:[10–11]

$$\mathrm{GO\ (s) + H^+ + \ e^- \longrightarrow ERGO\ (s) + H_2O} \quad (1)$$

According to Equation 2, the area of the reduction peak can be used to calculate the number of electrons transferred and thus, the approximate number of protons transferred. With n = number of transferred moles of electrons, Q = total charge obtained from the reduction peak, F=Faraday constant and z = number of electrons exchanged per oxygen group.

$$n = \frac{Q}{zF} \quad (2)$$

Previous studies on the mechanism of the electrochemical reduction of GO membranes revealed that three phases are involved, which are exposed to relevant interfaces. Accordingly, the electrochemical reduction process is explained by a three-phase interface (3PI) model, accounting for interfaces of GO-substrate-electrolyte and the electroformed interface GO-ERGO-electrolyte.[10,12] In Figure 1A, the evolution of the ERGO is depicted, based on the two 3PI models.

In the electrochemical reduction of GO membranes, electron conduction determines the electrochemical reduction process.[10,12b] However, the 3PI model was previously

[*] Dr. Y. Wang
College of Chemistry and Chemical Engineering
Yantai University
Shandong 264010, P. R. China
E-mail: yiqingwang@ytu.edu.cn
Prof. Dr. S. Eigler
Institute of Chemistry and Biochemistry
Freie Universität Berlin
Altensteinstraße 23a, 14195 Berlin, Germany
E-mail: siegfried.eigler@fu-berlin.de

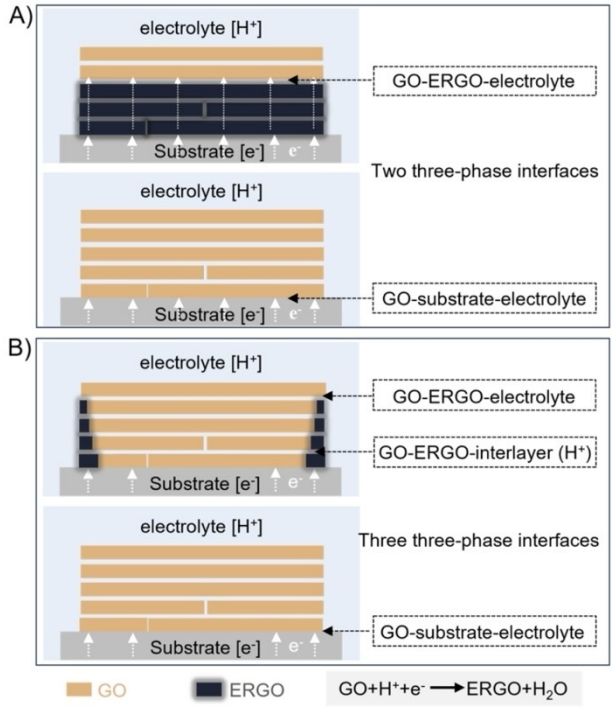

Figure 1. A) Electrochemical reduction reaction of GO membranes at two three-phase interfaces.[10,12] B) The electrochemical reduction of GO membrane at three three-phase interfaces influenced by proton permeability in this work. Schematic of the electrochemical reduction process for GO membranes to ERGO membranes on conductive substrate in electrolyte.

proposed in the study of the Fray-Farthing-Chen (FFC) Cambridge process and referred to a solid oxide (insulator)/solid metal (conductor)/molten salt (electrolyte) interface.[13] Therefore, although the 3PI model can be applied to explain the reduction of GO membranes, the two 3PI models does not fully account for the chemistry of GO and it does not account for the anisotropy of proton-conductivity, which determines the reduction process of GO.

Here, we consider the proton permeability of GO membranes and based on interfacial reactions identify proton-dominated electrochemical reduction processes, which proceed at three three-phase interfaces in the electrolyte (3–3PI, Figure 1B). Interpretation of the electrochemical reduction of GO based on 3–3PI models, through-plane channels with low tortuosity similar to the vertical edge of GO membranes can be identified and quantified. Accordingly, applying voltammetry and chronoamperometry in a three-electrode system combined with operando imaging of optical changes in contrast of the membrane surface allows to identify and quantify through-plane proton channels.

The preparation of GO is described in Supporting Information and based on our previous work.[14] As shown in Figure S1A and B, GO monolayers are deposited on 300 nm Si/SiO_2 wafers and the lateral dimension of GO is 15.1 μm. Average Raman spectra of GO monolayers are shown in Figure S2A. The relation of the I_D/I_G ratio and the full-width at half-maximum (Γ) of the main Raman modes and the distance of defects (L_D) in Figure S2B is based on the model introduced by Lucchese and co-workers.[15] The corresponding equations are used to derive L_D in SI. Figure S2C illustrates the XPS survey spectra of GO. The C/O ratio of GO is 2.2. A typical three-electrode cell suitable for materials studies includes a reference electrode, a counter electrode, and a working electrode, as shown in Figure S3. High concentrations (5 mg/ml) of GO are dropped on the surface of glassy carbon electrode (GCE) to avoid the coffee ring effect during the drying process.[11b] Electrochemical reduction of GO membranes with voltammetry and monitoring of membrane color change on the surface of the working electrode with a camera. The peak current of the reversible and irreversible voltammogram is given by Equation 1 and 2 in SI.[16] Proton transport can be analyzed based on the currents of the reduction peaks, whether the electrochemical reduction of GO is considered reversible or irreversible.[12a]

Voltammograms obtained from the electrochemical reduction of GO scanned over the full range from 0 V to −1.7 V are shown in Figure 2A and magnified as shown in Figure 2B. The loading of GO is approximately 20 μg. The membrane thickness is about 6.8 μm based on the membrane thickness conversion in Figure S4. The electrolyte is Ar-saturated phosphate buffer (PB) at pH 7.4 and the scan rate is 10 $mV\,s^{-1}$. Video S1 shows the color change of the membrane surface on the GCE. The inset images in Figure 2A show the color change of the membrane surface at potentials of −1.20, −1.40, −1.50, −1.55, −1.60, −1.65, and −1.70 V, respectively. Based on the electrochemical reduction peaks and the real-time changes in the membrane surface, the following results can be deduced. The first peak shown in Figure 2B reflects the reduction reaction at the GO-substrate-electrolyte (GSE) interface, which corresponds to the process shown in Figure 2C to 2D. In this initial reaction, protons are transported directly from the electrolyte and electrons are transferred directly from the GSE, so the first reduction peak is at a lower potential, and the onset potential of the first reduction peak is about −0.60 V vs. Ag/AgCl. The second peak reflects the reaction at the GO-ERGO-electrolyte (GEE) interface, corresponding to the process shown in Figures 2D through 2E. In this process, protons are transported directly from the electrolyte. Electrons, however, are transferred through ERGO, which has a higher resistance than GCE substrates. We hypothesize that the protons contact the electrochemical interface of GO, creating "electron traps". The process takes place in the through-plane direction at the edge of the membrane. The blue area curve (maximum peak) represents the electron and proton transfer at the GO-ERGO interlayer (GEI) interface according to the process shown in Figure 2D to 2G. In the interlayer, adsorbed water molecules can generate protons through self-dissociation, and oxygen functional groups in GO as hydrophilic sites attract interlayer protons.[1,17] Therefore, the protons required for the GO reduction process come from the interlayers and the electrons are conducted through ERGO. The electrochemical reduction reaction at this interface makes the reduction process slower and requires a higher potential than the

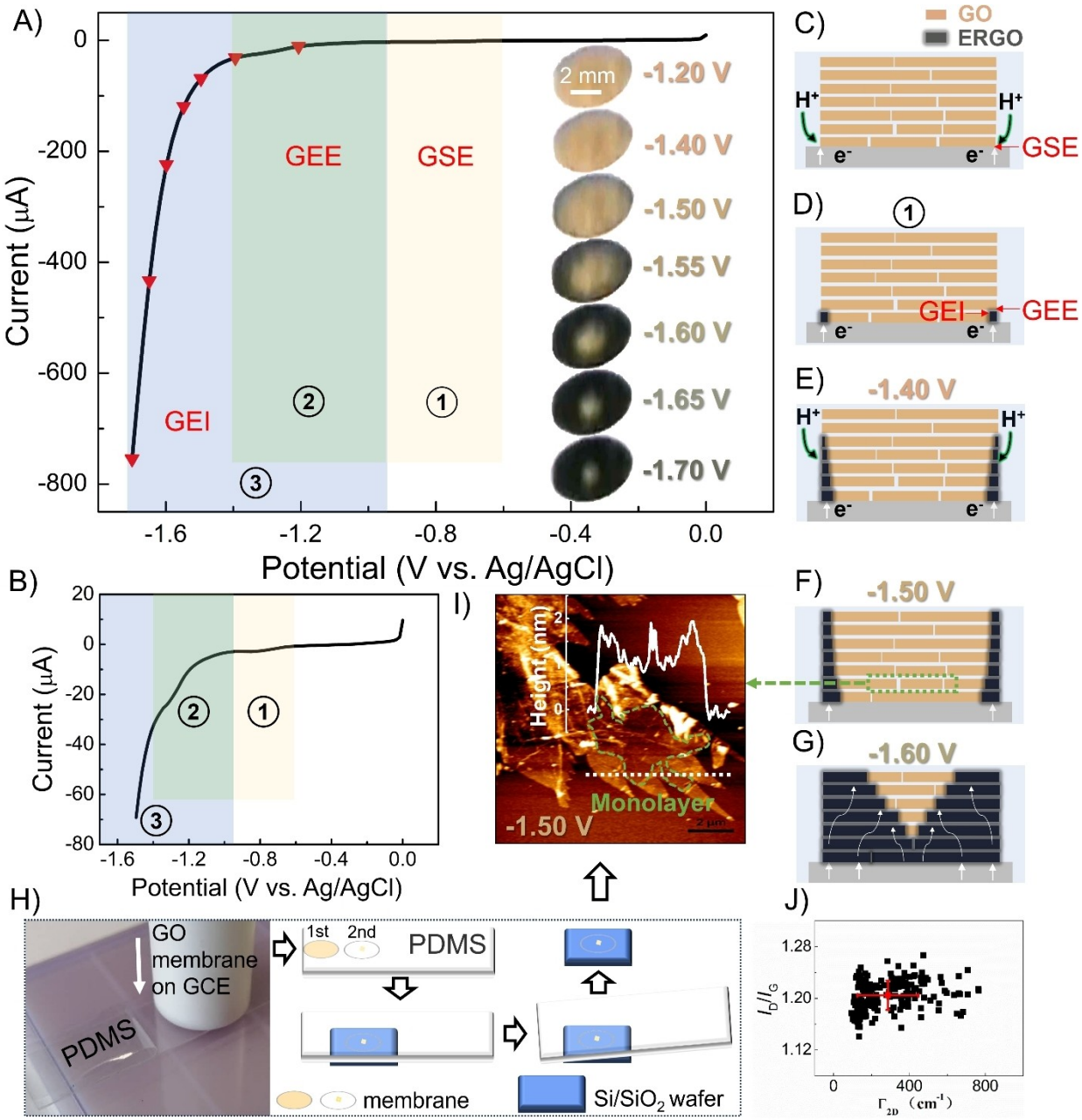

Figure 2. A) Voltammograms (0 to −1.7 V) of GO reduction. The insets show the membrane images when the potential was applied to −1.20, −1.40, −1.50, −1.55, −1.60, −1.65, and −1.70 V, respectively. Curves in different color areas reflect proton and electron transfer at different interfaces. B) Zoom in voltammograms of GO reduction. C) The state of the membrane prior to the appearance of the first peak in Figure 2A and 2B (at about −0.60 V). D) The state of the membrane after the appearance of the first peak. Changes in membrane at potentials of −1.40 V (E), −1.50 V (F), −1.60 V (G). H) Illustration of the process to obtain monolayers near the bottom of stacked membranes (−1.50 V). I) AFM images of monolayers near the bottom of stacked membrane that was reduced to −1.50 V deposited on 300 nm Si/SiO_2 wafers. J) Statistical Raman analysis of monolayers near the bottom of stacked membranes (−1.50 V) deposited on 300 nm Si/SiO_2 wafers.

previous two interfaces due to insufficient proton transport and electron conductivity through ERGO.[18] Although the electrochemical reduction reaction at this (GEI) interface makes the reduction process slower, the amount of this type of interface is larger than the others and therefore shows larger currents at large potential. The vertical edges of stacked GO membranes can be considered as through-plane channels. The GSE and GEE interfaces are the interfaces of the through-plane channels. From the above phenomena, it is clear that there are no through-plane channels in this stacked GO membrane except the vertical edges, although protons can be transported through defect-free monolayers of graphene.[3a,19]

The electrochemical reduction reaction process of GO membranes was verified by peeling monolayers in the electrochemical reduction of GO membranes and determin-

ing the reduction of monolayers by statistical Raman characterization. Reliable Raman analysis of graphene oxide requires monolayer flakes.[9,20] Therefore, we peeled off the monolayer near the bottom of the stacked membrane after the electrochemical reduction reaction at −1.50 V (Figure 2F). The method of obtaining the monolayer is shown in Figure 2H. The stacked membrane loaded on the GCE was pressed onto the PDMS stamp and then quickly peeled off, followed by a second pressing and peeling. The membrane material remaining on the PDMS after the second peel was pressed onto a 300 nm Si/SiO_2 wafer and then quickly peeled off to find the monolayer in the center of the membrane contour on the wafer.[9] Atomic force microscopy (AFM) images of monolayers are shown in Figure 2I. Statistical Raman spectroscopy of the monolayer was performed and Figure 2J shows that the I_D/I_G of the monolayer is 1.20, which is within the I_D/I_G range of GO. And the I_D/I_G of the ERGO monolayer is 1.82 (Figure S2B). Comparison of the of defect distance (L_D) values shows that GO has a smaller L_D than ERGO, suggesting that ERGO has a smaller defect density, which is attributed to the removal of oxygen defects by electrochemical reduction. In addition, the contact angle of the membrane left on the electrode after PDMS treatment was tested. The contact angle was 33.0° (Figure S5A). And the contact angle of the ERGO is 67.8° (Figure S5B). Based on the results, when the voltage is applied to −1.50 V using voltammetry, the monolayer near the bottom of the membrane is not electrochemically reduced. Thus, the changes to the membrane illustrated in Figure 2E to 2F are supported.

We further reduced the GO loading on the GCE to observe the electrochemical reduction of thinner membranes. The GO loading is approximately 10 μg. The membrane thickness is about 3.4 μm based on the membrane thickness conversion in Figure S4. Voltammograms obtained from the electrochemical reduction of GO scanned over the full range from 0 V to −1.5 V are shown in Figure 3A and enlarged in Figure 3B. Membrane changes are better observed at a low scanning rate (10 mV s^{-1}). The inset images in Figure 3A show the color change of the membrane surface at the potential of −0.90, −1.15, −1.20, −1.30 V, respectively. The first peak shown in Figure 3A and 3B reflects the transfer of electrons and protons at the GSE interface, corresponding to the phenomenon shown in Figure 3C. The reduction peak 1 represented by the initial reaction has the same onset potential (−0.6 V vs. Ag/AgCl) as in Figure 2B. In this process, protons are transported directly from the electrolyte and electrons are transferred directly from the GCE. It's striking that the area of the initial reaction peak 1 (the first peak) in Figure 3B is much larger than that of peak 1 in Figure 2B. According to Equations 1 and 2, the number of protons involved in the reaction can be deduced from the area of the reduction peak. More through-plane channels mean more initial reaction interfaces. Therefore, the number of through-plane channels of the GO membranes in Figure 3B is higher than that of the GO membrane with only vertical edges in Figure 2. With scanning to −1.15 V, we observe that a portion of the membrane surface turns black at the same

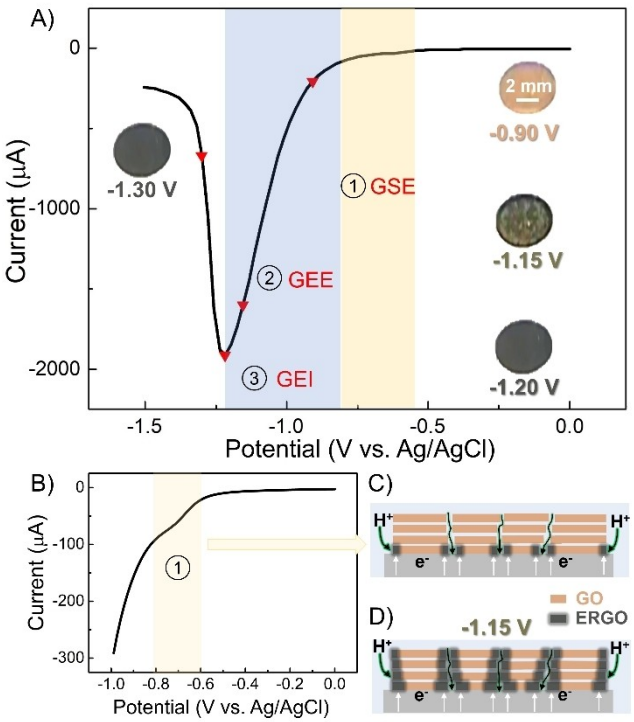

Figure 3. A) Voltammograms (0 to −1.5 V) of GO reduction. Inset membrane images at the potential of −0.90, −1.15, −1.20, −1.30 V, respectively. Curves in different color areas reflect proton and electron transfer at different interfaces. B) Zoom in cyclic voltammograms of GO reduction. C) The state of the membrane after the initial reaction. D) Changes in membrane at potentials of −1.15 V.

time as the vertical edge of the membrane, as shown in the inset of Figure 3A and Video S2. However, a portion of the membrane surface turns black at the same time as the edges, further indicating that there are through-plane channels except for the vertical edges of the membrane.

Pores associated with folding (Figure S4) and gaps in the drop-coated membrane, as well as vacancy defects in the flakes (Figure S2D), may be the origin of through-plane channels. In this process, the transfer of protons and electrons at the GEE interface corresponds to the phenomenon shown in Figure 3D. Protons are transported from the electrolyte and electrons are transferred by ERGO. In contrast to the three reduction peaks in Figure 2B, there are two reduction peaks in Figure 3A. The reduction peak of the GEE interface reaction is superimposed on the peak of the GEI interface reaction. As shown in Figure 3D, due to the presence of through-plane channels, more GEI interfaces react as the GEE interface reaction proceeds. The two interfacial reactions occur simultaneously and it is difficult to distinguish the respective reduction peaks. For a thin membrane, cyclic voltammetry features are subtle, and it is difficult to quantify membrane through-plane channels or anisotropy. However, we also used the chronoamperometry method in conjunction with real-time imaging to investigate the amount of through-plane channels in the membrane (Figure S7–8). Therefore, 150 μg of GO were drop-coated on the surface of the electrode with a length of 1 cm

(Figure S7). The *I-t* curve of the electrochemical reduction of the GO membrane was obtained by chronoamperometry. The applied voltage was −1.4 V *vs.* Ag/AgCl. Combined with real-time imaging, the range from the start of the reaction to the inflection point 1 was determined to be the curve represented by the GEE and GSE interface reaction. This is consistent with the phenomenon shown in Figure 2. There are no efficient through-plane channels such as membrane edges. In Figure S8, 5 μg of GO were drop-coated on the surface of the 1 cm electrode to obtain a thinner membrane. To make it easier to see the color difference, the drop-coated membrane is partially thicker. Similarly, the area from the start of the response to the inflection point 1 was determined to be the curve represented by the GEE and GSE interfacial response. This is the curve corresponding to the interfacial reaction of efficient continuous channels. The areas corresponding to the different reaction phases of the *I-t* curve represent the number of channels. Thus, the ratio of efficient through-plane channels to all channels for this membrane was about 44.2 %. For thicker membranes, there are wrinkles in the through-plane direction (Figure S4). The density of void defects in the monolayer of the membrane remains constant. Some holes formed by gaps and wrinkles in the through-plane direction are easily blocked with increasing membrane thickness. It can be hypothesized that the holes formed by gaps and folds in the through-plane direction are the main source of efficient low-tortuosity through-plane channels.

The interfacial reactions of through-plane channels by voltammetry are summarized in Figure 4. The initial reaction occurs at the GSE interface with an onset potential of −0.6 V vs. Ag/AgCl. Next, we investigated effects resulting from the size of flakes (Figure 4B). GO_{10s} was obtained after sonication of GO for 10 seconds with lateral dimensions of 2.7 μm (Figure S1C and D). GO_{30s} was obtained after 30 seconds with lateral dimension of 1.6 μm (Figure S1E and F). The investigated loadings are all 6 μg. We find that the onset potentials of the initial reaction interfaces are all -0.6 V. The reduction peaks, which correspond to the initial interfacial reactions are shown as colored labels of Figure 4B. By comparing the reduction peak areas corresponding to the initial interfacial reactions, the ratios of the amount of through-plane channels are 1 : 1.8 : 2.1 corresponding to GO, GO_{10s}, and GO_{30s} (Figure S6). The through-plane channels increase as the flake size decreases. The smaller the flakes, the more edges of flakes and sheet-sheet junctions are formed. It is further verified that the through-plane channels of the drop-cast membrane mainly originate from the gaps and holes formed by the irregular stacking of nanosheets.

It is important to note that a series of previous reports on the reduction of different species of oxygen groups at different potentials in the electrochemical reduction of GO need to be revisited because proton transport as an important factor affects the reduction process. GO has been characterized before and does not contain many carbonyl groups or other groups, which require high reduction potentials.[10,12b] However, hindered proton transfer processes lead to overpotential.

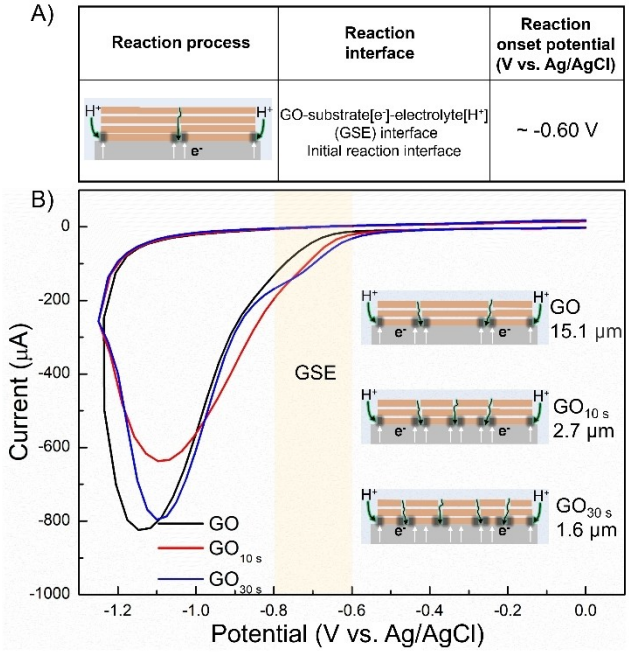

Figure 4. A) Electrochemical reduction reactions at initial reaction interfaces. B) Cycle voltammograms obtained from electrochemical reduction of different size of GO scanned over the full range of 0 to 1.25 V; The loading of the GCE is 6 μg. Conditions: supporting electrolyte: in Ar-saturated PB at pH 7.4; Scan rate: 100 mV s^{-1}. All starting potentials are at 0.0 V relative to the Ag/AgCl reference electrode.

Electrochemical reduction of GO is a common method to obtain reduced GO. In this work, we discovered three three-phase interfacial electrochemical reduction reactions dominated by protons. Based on the results, we propose a method to identify and quantify through-plane channels of GO proton membranes using electrochemical techniques and real-time imaging (Figure S9). First, the presence of through-plane channels is determined by real-time imaging. The ratio of through-plane channels on GO with different flake-size is determined to 1 : 1.8 : 2.1, corresponding to GO, GO_{10s}, and GO_{30s}, based on the reduction peaks of the initiated reactions obtained by cyclic voltammetry. Further chronoamperometry was combined with real-time imaging to obtain the amount of through channels or anisotropy in the membranes. This work provides a simple method to identify and quantify through-plane channels in stacked GO membranes in a three-electrode system. By comparing the amount of through-plane channels in GO membranes with different loadings and GO membranes composed of GO monolayers of different sizes, it is hypothesized that the through-plane channels of the drop-cast membrane mainly originate from gaps and holes formed by irregular stacking of nanosheets.

Supporting Information

The authors have cited additional references within the Supporting Information.[9,14b,15–16,20]

Acknowledgements

This work is supported by the Young Scholars Research Fund of Yantai University (HY22B127). Open Access funding enabled and organized by Projekt DEAL.

Conflict of Interest

The authors declare no conflict of interest.

Data Availability Statement

The data that support the findings of this study are available in the supplementary material of this article.

Keywords: Three-phase interface · graphene oxide proton membranes · through-plane channel

[1] M. R. Karim, K. Hatakeyama, T. Matsui, H. Takehira, T. Taniguchi, M. Koinuma, Y. Matsumoto, T. Akutagawa, T. Nakamura, S. Noro, T. Yamada, H. Kitagawa, S. Hayami, *J. Am. Chem. Soc.* **2013**, *135*, 8097–8100.

[2] a) I. Sahroni, T. Kodama, M. S. Ahmad, T. Nakahara, Y. Inomata, T. Kida, *Nano Lett.* **2024**, *24*, 3590–3597; b) S. K. Green, J. Lee, H. J. Kim, G. A. Tompsett, W. B. Kim, G. W. Huber, *Green Chem.* **2013**, *15*, 1869–1879.

[3] a) S. Hu, M. Lozada-Hidalgo, F. C. Wang, A. Mishchenko, F. Schedin, R. R. Nair, E. W. Hill, D. W. Boukhvalov, M. I. Katsnelson, R. A. W. Dryfe, I. V. Grigorieva, H. A. Wu, A. K. Geim, *Nature* **2014**, *516*, 227–230; b) L. Chen, G. Shi, J. Shen, B. Peng, B. Zhang, Y. Wang, F. Bian, J. Wang, D. Li, Z. Qian, G. Xu, G. Liu, J. Zeng, L. Zhang, Y. Yang, G. Zhou, M. Wu, W. Jin, J. Li, H. Fang, *Nature* **2017**, *550*, 380–383; c) R. K. Joshi, P. Carbone, F. C. Wang, V. G. Kravets, Y. Su, I. V. Grigorieva, H. A. Wu, A. K. Geim, R. R. Nair, *Science* **2014**, *343*, 752–754; d) X. Qian, L. Chen, L. Yin, Z. Liu, S. Pei, F. Li, G. Hou, S. Chen, L. Song, K. H. Thebo, H.-M. Cheng, W. Ren, *Science* **2020**, *370*, 596–600; e) L.-H. Xu, S.-H. Li, H. Mao, Y. Li, A.-S. Zhang, S. Wang, W.-M. Liu, J. Lv, T. Wang, W.-W. Cai, L. Sang, W.-W. Xie, C. Pei, Z.-Z. Li, Y.-N. Feng, Z.-P. Zhao, *Science* **2022**, *378*, 308–313; f) P. R. Kidambi, P. Chaturvedi, N. K. Moehring, *Science* **2021**, *374*, eabd7687; g) Y. Xia, H. Cao, F. Xu, Y. Chen, Y. Xia, D. Zhang, L. Dai, K. Qu, C. Lian, K. Huang, W. Xing, W. Jin, Z. Xu, *Nature Sustainability* **2022**, *5*, 1080–1091.

[4] T. Bayer, R. Selyanchyn, S. Fujikawa, K. Sasaki, S. M. Lyth, *J. Membr. Sci.* **2017**, *541*, 347–357.

[5] K. Hatakeyama, M. R. Karim, C. Ogata, H. Tateishi, A. Funatsu, T. Taniguchi, M. Koinuma, S. Hayami, Y. Matsumoto, *Angew. Chem. Int. Ed.* **2014**, *53*, 6997–7000.

[6] H. Tateishi, K. Hatakeyama, C. Ogata, K. Gezuhara, J. Kuroda, A. Funatsu, M. Koinuma, T. Taniguchi, S. Hayami, Y. Matsumoto, *J. Electrochem. Soc.* **2013**, *160*, F1175–F1178.

[7] a) H. Liu, X. Huang, Y. Wang, B. Kuang, W. Li, *Nat. Commun.* **2024**, *15*, 164; b) H. G. Zhang, X. Quan, L. Du, G. L. Wei, S. Chen, H. T. Yu, Y. C. Dong, *Proc. Natl. Acad. Sci. USA* **2023**, *120*, e2219098120; c) M. Liu, P. J. Weston, R. H. Hurt, *Nat. Commun.* **2021**, *12*, 507; d) D. Wu, M. Sun, W. Zhang, W. Zhang, *ACS Appl. Mater. Interfaces.* **2023**, *15*, 52029–52037.

[8] a) S. Sy, G. Jiang, J. Zhang, H. Zarrin, T. Cumberland, S. Abureden, E. Bell, J. Gostick, A. Yu, Z. Chen, *ACS Nano* **2020**, *14*, 14947–14959; b) W. H. Zhang, M. J. Yin, Q. Zhao, C. G. Jin, N. Wang, S. Ji, C. L. Ritt, M. Elimelech, Q. F. An, *Nat. Nanotechnol.* **2021**, *16*, 337–343.

[9] Y. Wang, F. Grote, Q. Cao, S. Eigler, *J. Phys. Chem. Lett.* **2021**, *12*, 10009–10014.

[10] A. A. Zhou, J. Bai, W. Hong, H. Bai, *Carbon* **2022**, *191*, 301–332.

[11] a) J. A. Quezada-Renteria, C. O. Ania, L. F. Chazaro-Ruiz, J. R. Rangel-Mendez, *Carbon* **2019**, *149*, 722–732; b) Y. Wang, S. Eigler, *Phys. Chem. Chem. Phys.* **2022**, *24*, 8076–8080.

[12] a) M. Zhou, Y. Wang, Y. Zhai, J. Zhai, W. Ren, F. Wang, S. Dong, *Chem.* **2009**, *15*, 6116–6120; b) A. Ambrosi, C. K. Chua, N. M. Latiff, A. H. Loo, C. H. Wong, A. Y. Eng, A. Bonanni, M. Pumera, *Chem. Soc. Rev.* **2016**, *45*, 2458–2493.

[13] G. Z. Chen, E. Gordo, D. J. Fray, *Metal. Mater. Trans. B* **2004**, *35*, 223–233.

[14] a) Y. Wang, C. Neumann, M. Hußmann, Q. Cao, Y. Hu, O. Garrity, P. Kusch, A. Turchanin, S. Eigler, *Adv. Mater. Inter.* **2021**, *8*, 2100783; b) S. Eigler, M. Enzelberger-Heim, S. Grimm, P. Hofmann, W. Kroener, A. Geworski, C. Dotzer, M. Rockert, J. Xiao, C. Papp, O. Lytken, H. P. Steinruck, P. Muller, A. Hirsch, *Adv. Mater.* **2013**, *25*, 3583–3587.

[15] L. G. Cancado, A. Jorio, E. H. Ferreira, F. Stavale, C. A. Achete, R. B. Capaz, M. V. Moutinho, A. Lombardo, T. S. Kulmala, A. C. Ferrari, *Nano Lett.* **2011**, *11*, 3190–3196.

[16] a) H. Yamada, K. Yoshii, M. Asahi, M. Chiku, Y. Kitazumi, *Electrochemistry* **2022**, *90*, 102005–102005; b) J. F. Rusling, S. L. Suib, *Adv. Mater.* **1994**, *6*, 922–930.

[17] a) K. D. J. C. O. M. Kreuer, *Chem. Mater.* **1996**, *8*, 610–641; b) J. Wang, L. Zhao, D. Wei, W. Wu, J. Zhang, X. Cheng, *Ind. Eng. Chem. Res.* **2016**, *55*, 11931–11942; c) K. W. Silverstein, C. E. Halbig, J. S. Mehta, A. Sharma, S. Eigler, J. M. Mativetsky, *Nanoscale* **2019**, *11*, 3112–3116.

[18] A. Ge, G. Kastlunger, J. Meng, P. Lindgren, J. Song, Q. Liu, A. Zaslavsky, T. Lian, A. A. Peterson, *J. Am. Chem. Soc.* **2020**, *142*, 11829–11834.

[19] L. Mogg, S. Zhang, G. P. Hao, K. Gopinadhan, D. Barry, B. L. Liu, H. M. Cheng, A. K. Geim, M. Lozada-Hidalgo, *Nat. Commun.* **2019**, *10*, 4243.

[20] A. C. Ferrari, D. M. Basko, *Nat. Nanotechnol.* **2013**, *8*, 235–246.

Manuscript received: July 5, 2024
Accepted manuscript online: September 17, 2024
Version of record online: October 31, 2024